Concluding Remarks

We have reported the first ab initio theoretical study of a "realistic" transition-metal–carbene complex, $(CO)_3NiCH_2$. Predictions of its geometrical characteristics were reinforced by a "benchmark" optimization of the $Ni(CO)_4$ complex which was experimentally determined. The findings are for the most part consistent with geometrical and electronic expectations for this important class of organometallic species. This work suggests a variety of further studies to follow, for example, directly comparing the prototype chromium and iron carbenes (2) and (3) or replacing one carbene hydrogen with an OR or NR_2 ligand of the type found in Fischer carbenes. From a theoretical perspective it will also be important to directly assess the importance of correlation effects on predicted transition-metal carbene properties. Needless to say, the experimental determination of the structure and the photoelectron spectra of $(CO)_3NiCH_2$ or related prototype carbenes would be of great help in further confirming the reliability of the theoretical techniques used here.

Acknowledgment. We thank Professor J. Demuynck, Professor A. Veillard, and Professor M. Hall for helpful discussions. This work was supported in part by the Division of Basic Energy Sciences of the U.S. Department of Energy (Contract W-7405-ENG-48) and the National Science Foundation (Grant CHE-7721305).

Novel Method for Angle Determinations by EXAFS via a New Multiple-Scattering Formalism

Boon-Keng Teo

Contribution from Bell Laboratories, Murray Hill, New Jersey 07974.
Received October 31, 1980

Abstract: A new EXAFS formulation which takes into account the effect of multiple scattering has been developed. Theoretical scattering amplitude and phase functions have been calculated for various scattering angles. Combining the new multiple-scattering formalism and the new theoretical functions enables the unraveling of the "focusing" effect as well as assessment of the relative importance of various multiple-scattering pathways as the scattering angle varies. On this basis, a novel method for interatomic angle determinations by EXAFS is devised and applied to a few known systems to illustrate the usefulness and accuracy of the technique. The accuracy for angle determination is better than 6% for low Z ($Z \leq 10$) and 3% for high Z scatterers. In most cases, it amounts to an accuracy of better than ca. 5°, which is comparable to the scattered range of crystallographically independent bond angles often observed in diffraction studies. The method requires no single-crystal measurements and is applicable to wide varieties of samples (polycrystalline or amorphous solids, liquids and solutions, gases, surfaces, polymers, etc.). This work also provides the first evidence that multiple-scattering processes can be important in determining the EXAFS of distant shells, especially at large bond angles.

The phenomenon of extended X-ray absorption fine structure (EXAFS) refers to the oscillatory modulation of the X-ray absorption coefficient as a function of X-ray photon energy beyond the absorption edge. The existence of such an extended fine structure has been known for a long time,[1] however, it is not until recently that the short-range single-electron single-scattering theory was formulated, particularly through the work of Sayers, Stern, and Lytle,[2] which led to the recognition of its structural content. For the past few years, the availability of synchrotron radiation[3] has made EXAFS spectroscopy a practical structural tool. It is particularly useful for complex or unstable chemical or biological systems where conventional diffraction methods are not applicable and/or single crystals are not available.

There are two advantageous characteristics of EXAFS spectroscopy which make it a powerful structural technique. First, being sensitive to short-range order in atomic arrangements rather than long-range crystalline order, it can focus on the *local* environment of *specific* X-ray absorbing atoms, one at a time. This allows accurate structural determination of the active site of a complex system. Second, since EXAFS signal attenuates rapidly beyond first and second coordination shells, it greatly simplifies the interpretation of the data.[4]

The major weakness of EXAFS spectroscopy is that it does not provide full stereochemical details. It gives only local structures in terms of radial distributions (distances) about the absorbing atoms. No *direct* method of determining angular information is hitherto available, except, perhaps, for elaborate measurements on single crystals by utilizing polarized X-rays.[5] In principle, though, one can argue that bond angles can be calculated if enough interatomic distances are known from EXAFS measurements of different absorbers within the same molecule. However, this indirect angle determination method is often not feasible, since not all the atoms involved are convenient X-ray absorbers (viz. the energies of their absorption edges may not be easily accessible). Furthermore, the very same advantageous characteristics of EXAFS (short range, single scattering) are also its serious limitations: distance determinations can be made out to only ca. 4 Å. The situation, however, changes dramatically when atoms (including the X-ray absorbing atom and its neighbors) are arranged in a linear or nearly collinear fashion. In such cases, EXAFS con-

(1) R. de L. Kronig, *Z. Phys.*, **70**, 317 (1931); **75**, 191, 468 (1932).
(2) (a) D. E. Sayers, E. A. Stern, and F. W. Lytle, *Phys. Rev. Lett.*, **27**, 1204 (1971); (b) E. A. Stern, *Phys. Rev. B*, **10**, 3027 (1974); (c) E. A. Stern, D. E. Sayers, and F. W. Lytle, *ibid.*, **11**, 4836 (1975), and references cited therein.
(3) (a) H. Winick and A. Bienenstock, *Annu. Rev. Nucl. Part. Sci.*, **28**, 33 (1978); (b) B. M. Kincaid and P. Eisenberger, *Phys. Rev. Lett.*, **34**, 1361 (1975); (c) R. E. Watson and M. L. Perlman, *Science (Washington, DC)*, **199**, 1295 (1978); (d) B. W. Batterman and N. W. Ashcroft, *ibid.*, **206**, 157 (1979).
(4) For reviews, see (a) E. A. Stern, *Contemp. Phys.*, **19**, 289 (1978); (b) P. Eisenberger and B. M. Kincaid, *Science (Washington, DC)*, **200**, 1441 (1978); (c) R. G. Shulman, P. Eisenberger, and B. M. Kincaid, *Annu. Rev. Biophys. Bioeng.*, **7**, 559 (1978); (d) D. R. Sandstrom and F. W. Lytle, *Annu. Rev. Phys. Chem.*, **30**, 215 (1979); (e) "Synchrotron Radiation Research", H. Winick and S. Doniach, Eds., Plenum, New York, 1980; (f) "EXAFS Spectroscopy: Techniques and Applications," B. K. Teo and D. C. Joy, Eds., Plenum, New York, 1981; (g) B. K. Teo, *Acc. Chem. Res.*, **13**, 412 (1980); (h) P. A. Lee, P. H. Citrin, P. Eisenberger, and B. M. Kincaid, *Rev. Mod. Phys.*, submitted for publication.
(5) (a) S. M. Heald and E. A. Stern, *Phys. Rev. B*, **16**, 5549 (1977); (b) L. I. Johansson and J. Stohr, *Phys. Rev. Lett.*, 43, 1882 (1979).

0002-7863/81/1503-3990$01.25/0

tributions from neighboring atoms as far as 8 Å can be observed. For these systems, both the amplitude and the phase of the EXAFS of a more distant neighbor are significantly affected by the intervening atom(s). In particular, the amplitude is greatly enhanced, and the effect is therefore commonly called "focusing" effect.[6] The single-scattering theory of EXAFS fails in these situations and one must take into account multiple-scattering processes involving the intervening atoms.[7-9]

This paper attempts to address both of these problems. Our goal is threefold. First, we would like to develop a new formulation of EXAFS which will take into account the effect of multiple scattering. This is described in the first section. In the second section, we will attempt to calculate the scattering amplitude and phase functions for any arbitrary scattering angle by using Lee and Beni's method.[10] We hope to understand the focusing effect with these theoretical functions. Finally, we would like to develop a novel method for determining bond *angles*, in addition to the interatomic *distances*, by EXAFS spectroscopy for unoriented materials. This technique is described in the third section with a few examples. It should be noted that this represents the first successful attempt in bond angle determination by EXAFS spectroscopy. The method requires no single-crystal measurements and is applicable to wide varieties of samples (polycrystalline or amorphous solids, liquids and solutions, gases, surfaces, polymers, etc). This work also provides the first evidence that multiple-scattering processes involving three atoms (including the absorber and two neighboring atoms) can be important in determining the EXAFS of the distant shells, especially at large bond angles. Multiple scatterings involving more than three atoms are likely to be of less importance due to the large effective total path lengths involved, except, perhaps, in cases where all the bond angles are close to linearity.

Multiple Scattering

The single-electron single-scattering theory[2,7,10] of EXAFS is given by

$$\chi(k) = \frac{\mu - \mu_0}{\mu_0} = \frac{(-1)^l}{k}\sum_j \frac{N_j}{r_j^2} e^{-2\sigma_j^2 k^2} e^{-2r_j/\lambda}\, \mathrm{Im}[\mathrm{f}(\pi,k) e^{i2kr_j} e^{i2\delta_l'(k)}] \tag{1}$$

where l is the angular momentum of the outgoing wave, and the orientation effect of the sample has been averaged over (i.e., spherically averaged). Strictly speaking, eq 1 is valid only for K or L_I edge were excitation of a s state produces a p state with $l = 1$. For L_{II} or L_{III} edges (excitation of a p state), the description of EXAFS is complicated by the fact that the initial p state can go to a final state of s ($l = 0$) or d ($l = 2$) symmetry, resulting in more than one term for each scatterer in eq 1. However, it has been shown from theoretical calculations[11] that transitions to the d final states are generally favored by a factor of 50 over the s final states such that eq 1 can still be used to describe $L_{II,III}$ edge EXAFS with $l = 2$. This conclusion is also supported by an elaborate study on the angular dependence of the W L_{III} edge EXAFS in single-crystal WSe_2.[5a]

In eq 1, $f(\pi,k)$ describes the *backscattering* from each of the N_j neighboring atoms (scatterers) of the jth type at a distance r_j away from the central atom (absorber). The Debye–Waller factor σ_j arises from the smearing effect due to thermal vibration (assumed to be harmonic) and static disorder (assumed to have a Gaussian distribution of distances). The term $e^{-2r_j/\lambda}$ is due to inelastic (scattering) losses with λ being the electron mean free path. The photoelectron wave vector k is defined as

$$k = [(2m/\hbar^2)(E - E_0)]^{1/2} \tag{2}$$

where E is the photon energy, E_0 is the energy threshold of the absorption edge, and m is the mass of an electron. If one approximates the spherical nature of the outgoing wave by a plane wave, the backscattering term is given by

$$\mathrm{f}(\pi,k) = \mathrm{F}(k) e^{i\theta(k)} \tag{3}$$

where $F(k)$ is the backscattering amplitude and $\theta(k)$ is the backscattering phase. Also included in eq 1 is the l phase shift $\delta_l'(k)$ due to the absorbing atom where $l = 1$ for K or L_I edge and $l = 2$ for L_{II} or L_{III} edge.[10,11]

For EXAFS data analysis, it is convenient to rewrite eq 1 as

$$\chi(k) = \sum_j N_j \mathrm{F}_j(k) e^{-2\sigma_j^2 k^2} e^{-2r_j/\lambda} \frac{\sin\,[2kr_j + \phi_j(k)]}{kr_j^2} \tag{4}$$

where, for each term

$$\phi(k) = \phi_a{}^l(k) + \phi_b(k) - l\pi \tag{5}$$

$$\phi_a{}^l(k) = 2\delta_l'(k) \tag{6}$$

$$\phi_b(k) = \theta(k) \tag{7}$$

Here $l = 1$ for K or L_I edges and $l = 2$ for L_{II} or L_{III} edges.[11]

The single-electron single-scattering theory (eq 1) of EXAFS makes use of the fact that in most cases, multiple scattering is not important.[12] This assumption is generally valid if one considers that multiple-scattering processes can be accounted for by adding all scattering paths that originate and terminate at the central atom (absorber). Each of these processes then behaves like $\sin(2kr_{\mathrm{eff}})$ where $2r_{\mathrm{eff}}$ is the total scattering path length which is much larger than that of the backscattering(s) from the nearest neighbors. Thus, multiple scatterings will give rise to rapidly oscillatory waves in k space which tend to cancel out. The amplitude of these waves are also significantly attenuated by the large scattering path lengths, making it relatively unimportant in comparison with the direct backscattering.[7]

On the other hand, multiple scattering in EXAFS can become important when atoms are arranged in an approximately collinear array. In such cases, the outgoing photoelectron is strongly *forward scattered* by the intervening atom, resulting in a significant amplitude enhancement. In fact, both the amplitude and the phase are modified by the intervening atom(s) for bond angles ranging from 180 to ~75°. The effect, however, drops off very rapidly for bond angles below ca. 150°. For these systems, it is necessary to modify the EXAFS theory so as to take into account multiple scattering involving the intervening atom(s). For the sake of convenience, let us consider a three-atom array A–B–C where A is the central atom (absorber), B is the nearest neighbor (the intervening atom), and C is the next nearest neighbor. The generalization of the following theory to more neighboring atoms is straightforward. For such a system, the EXAFS of the absorber A is composed of two contributions, one from the backscattering of B and the other from the backscattering of C with possible multiple scatterings via atom B. We shall designate these two contributions as AB and AC, respectively. These two contributions can generally be separated by Fourier filtering which involves (1) Fourier transforming the EXAFS data in k space to a radial distribution function in distance r space, (2) selecting the distance of interest with some smooth window, and (3) transforming the data back to k space. The two resulting Fourier filtered AB and AC EXAFS spectra correspond to the A–B and the A–C distances, respectively, in the radial distribution function. The former can be described quite adequately by the backscattering from the atom B with the single-electron single-scattering theory (eq 1). The latter, which is affected by multiple scattering involving the intervening atom B, must be treated with a generalized formulation as described below.

(6) This effect, which is analogous to an amplifying relay system, was first noticed in the fourth shell of copper and in nickel tetracarbonyl.[8]

(7) (a) P. A. Lee and J. B. Pendry, *Phys. Rev. B*, **11**, 2795 (1975); (b) C. A. Ashley and S. Doniach, *ibid.*, **11**, 1279 (1975).

(8) B. M. Kincaid, unpublished.

(9) G. Beni, P. A. Lee, and P. M. Platzman, *Phys. Rev. B*, **13**, 5170 (1976).

(10) P. A. Lee and G. Beni, *Phys. Rev. B*, **15**, 2862 (1977).

(11) B. K. Teo and P. A. Lee, *J. Am. Chem. Soc.*, **101**, 2815 (1979).

(12) Strictly speaking, the single-electron single-scattering theory of EXAFS already includes one particular multiple scattering pathway, viz., the backscattering process involving the central atom which gives rise to the $2kr$ phase factor. In this paper, multiple scatterings refer to processes involving atoms other than the central atom.

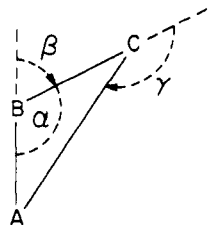

Figure 1. Schematic representation of a three-atom ABC system where A is the X-ray absorbing atom (central atom), B is the nearest neighbor, and C is the next nearest neighbor. Here α is the A–B–C bond angle and β and γ are scattering angles at atoms B and C, respectively.

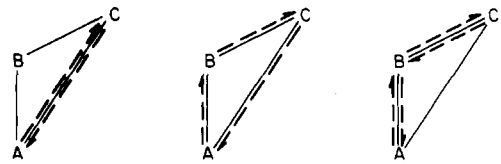

Figure 2. Schematic representation of three scattering pathways for a three-atom ABC system. Each of these pathways originates and terminates at the absorbing atom A. Pathway I is the direct backscattering from atom A to C and back. Pathway II is the multiple scattering via atom B around the triangle in either direction (only one is shown), and pathway III is the multiple scattering via atom B in both outgoing and incoming trips.

Let us first define a scattering angle β at atom B (and similarly γ at atom C) which is related to the bond angle A–B–C (α) (cf. Figure 1) by

$$\beta = 180 - \alpha \tag{8}$$

For any arbitrary angle β, the scattering at any atom B can be described by

$$f(\beta,k) = F(\beta,k)e^{i\theta(\beta,k)} \tag{9}$$

where $F(\beta,k)$ and $\theta(\beta,k)$ are the amplitude and phase functions, respectively. For *backscattering* where $\beta = 180° = \pi$ radians, eq 9 becomes eq 3 with $F(\pi,k) \equiv F(k)$ and $\theta(\pi,k) \equiv \theta(k)$ being the familiar backscattering amplitude and phase shifts tabulated in our previous paper.[11]

As mentioned earlier, multiple-scattering processes in EXAFS can be accounted for by summing contributions from all scattering pathways originating and terminating at the absorbing atom. For the simple three-atom system, the EXAFS contribution which corresponds to the A–C peak in the Fourier transform arises from three scattering pathways exemplified schematically in Figure 2. The first pathway (I) is the direct backscattering from A to C and back (viz., A → C → A). The second pathway (II) is the multiple scattering via atom B around the triangle in either directions (viz. A → B → C → A or A → C → B → A). This term should therefore be counted twice. The third pathway (III) is the multiple scattering via the intervening atom B on both outgoing and incoming trips (via. A → B → C → B → A). The AC EXAFS, corresponding to the A–C distance, is then the sum of these three terms:

$$\chi^{AC}(k) = \frac{(-1)^l}{k}e^{-2\sigma_C^2k^2}\,\mathrm{Im}\left[e^{2i\delta_l'(k)}\left(\frac{f_C(\pi,k)}{r_{AC}^2}e^{-2r_{AC}/\lambda}e^{i2kr_{AC}} + \frac{2f_B(\beta,k)f_C(\gamma,k)}{r_{AB}r_{BC}r_{AC}}e^{-2[(r_{AB}+r_{BC}+r_{AC})/2]/\lambda}e^{i2k[(r_{AB}+r_{BC}+r_{AC})/2]} + \frac{f_B(\beta,k)^2f_C(\pi,k)}{r_{AB}^2r_{BC}^2}e^{-2(r_{AB}+r_{BC})/\lambda}e^{i2k(r_{AB}+r_{BC})}\right)\right] \tag{10}$$

For relatively large γ, we can make the following approximation:

$$f_C(\gamma,k) \sim f_C(\pi,k) \tag{11}$$

We shall see in the next section that this is not an unreasonable approximation for $120 \lesssim \gamma \lesssim 180°$ (especially at high k values), which corresponds to the range of β where multiple scattering is important. Equation 10 then becomes

$$\chi^{AC}(k) = \frac{(-1)^l}{k}e^{-2\sigma_C^2k^2}\,\mathrm{Im}\left[e^{2i\delta_l'(k)}\frac{f_C(\pi,k)}{r_{AC}^2}e^{-2r_{AC}/\lambda}e^{i2kr_{AC}}\left(1 + \frac{r_{AC}}{r_{AB}r_{BC}}f_B(\beta,k)e^{-(r_{AB}+r_{BC}-r_{AC})/\lambda}e^{ik(r_{AB}+r_{BC}-r_{AC})}\right)^2\right] \tag{12}$$

If we now make the plane wave approximations

$$f_B(\beta,k) = F_B(\beta,k)e^{i\theta_B(\beta,k)} \tag{13}$$

$$f_C(\pi,k) = F_C(k)e^{i\theta_C(k)} \tag{14}$$

as well as define

$$\tilde{r} = r_{AC}/(r_{AB}r_{BC}) \tag{15}$$

$$\Delta r = r_{AB} + r_{BC} - r_{AC} \tag{16}$$

$$\tilde{\theta} = \theta_B(\beta,k) + k(\Delta r) \tag{17}$$

$$\Omega_B(\beta,k)e^{i\omega_B(\beta,k)} = [1 + \tilde{r}f_B(\beta,k)e^{-\Delta r/\lambda}e^{ik(\Delta r)}]^2 \tag{18}$$

we have

$$\chi^{AC}(k) = \left[\frac{(-1)^l}{k}\right]e^{-2\sigma_C^2k^2}e^{-2r_{AC}/\lambda}\left[\frac{F_C(k)}{r_{AC}^2}\right]\Omega_B(\beta,k) \times \mathrm{Im}(e^{i(2\delta_l'(k)+\theta_C(k)+\omega_B(\beta,k)+2kr_{AC})}) \tag{19}$$

or in the notation of eq 4

$$\chi^{AC}(k) = \Omega_B(\beta,k)F_C(k)e^{-2\sigma_C^2k^2}e^{-2r_{AC}/\lambda} \times \left(\frac{\sin[2kr_{AC} + \phi_{AC}(k) + \omega_B(\beta,k)]}{kr_{AC}^2}\right) \tag{20}$$

where $\phi_{AC}(k) = \phi_A^l(k) + \phi_C(k) - l\pi$.

It is apparent from eq 20 that the effect of multiple scattering via the intervening atom B is to multiply the amplitude $F_C(k)$ by $\Omega_B(\beta,k)$ and add $\omega_B(\beta,k)$ to the phase $\phi_{AC}(k)$. That is, if one substitutes the modified amplitude $F_C(k)\Omega_B(\beta,k)$ for $F_C(k)$ and the corrected phase $\phi_C(k) + \omega_B(\beta,k)$ for $\phi_C(k)$, the EXAFS data can be analyzed in the usual way. It is also clear that the treatment of multiple scattering in EXAFS can be generalized to include more scatterers and, whenever multiple scattering becomes important, the terms in eq 1 and 4 affected must be replaced by eq 19 and 20, respectively. Clearly, both $\Omega_B(\beta,k)$ and $\omega_B(\beta,k)$ are functions of the scattering angle β. Together they form the basis for bond angle determinations.

Equation 18 can be rewritten as

$$\Omega_B(\beta,k) = 1 + 2\tilde{r}F_B(\beta,k)e^{-\Delta r/\lambda}\cos\tilde{\theta} + [\tilde{r}F_B(\beta,k)e^{-\Delta r/\lambda}]^2 \tag{21}$$

$$\omega_B(\beta,k) = 2\tan^{-1}\left[\frac{\tilde{r}F_B(\beta,k)e^{-\Delta r/\lambda}\sin\tilde{\theta}}{1 + \tilde{r}F_B(\beta,k)e^{-\Delta r/\lambda}\cos\tilde{\theta}}\right] \tag{22}$$

It should be noted that the approximation implicit in eq 11 becomes exact as $\beta = 0°$ (i.e., linear case). However, at this extreme, one should in theory consider only the multiple scattering pathway III in Figure 2. As we shall see in a later section, in reality when the system approaches linearity, III becomes the dominant scattering pathway.

Throughout this paper, we chose to use the "experimental" unit of Å for all the amplitude functions, radian for all the phase functions, $Å^{-1}$ for the electron wave vector k, and eV for the energies.

Calculation of Scattering Amplitude and Phase

To calculate the scattering amplitude and phase of the photoelectron by an atom at any arbitrary angle β, we make use of the following equation[13]

$$f(\beta,k) = \frac{1}{k}\sum_{l=0}^{\infty}(2l+1)e^{i\delta_l(k)}\sin\delta_l(k)P_l(\cos\beta) \tag{23}$$

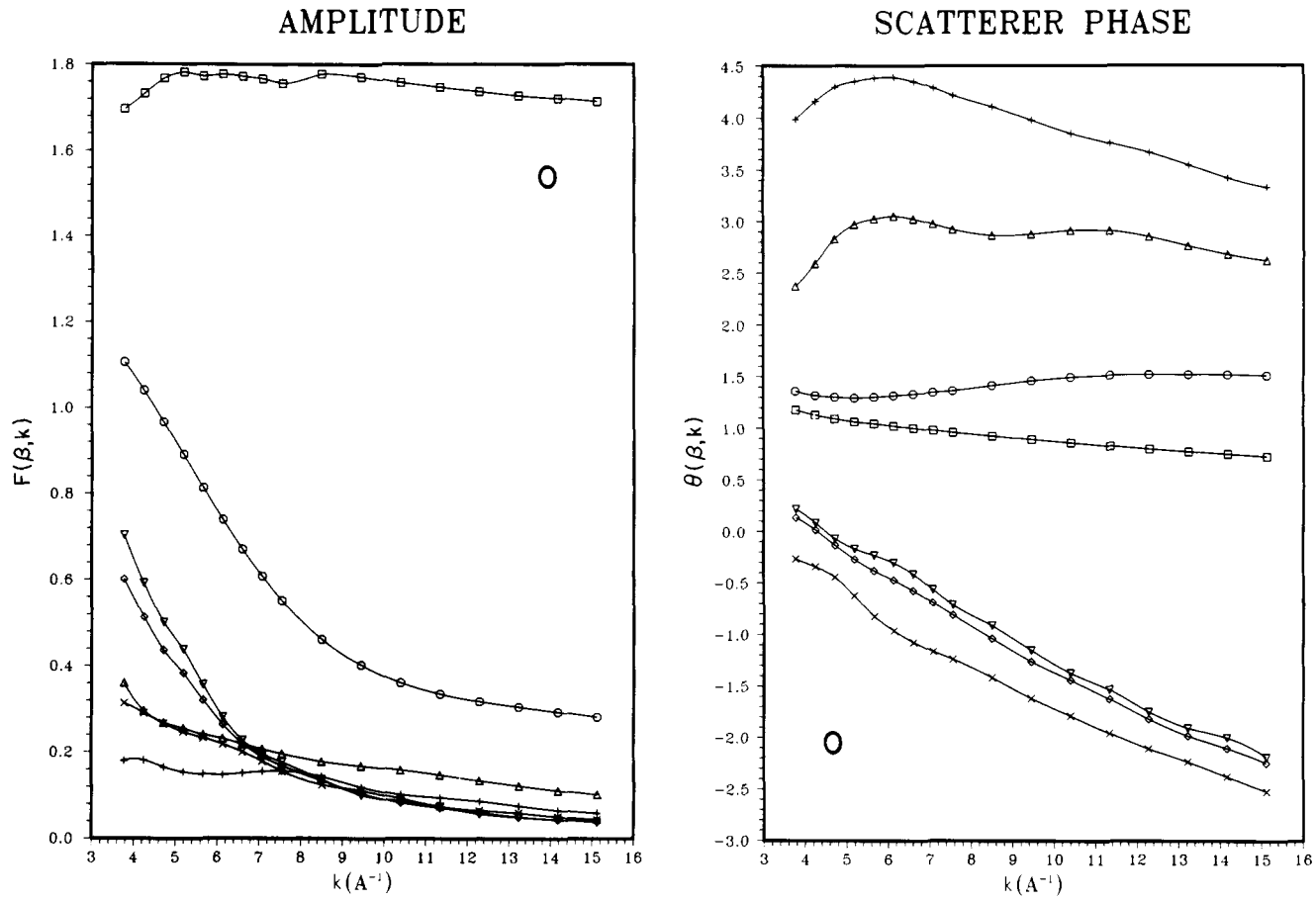

Figure 3. (a) Scattering amplitude $F(\beta,k)$ in Å vs. photoelectron wave vector k in Å^{-1} for oxygen at different scattering angles β where β = 0 (□), 30 (○), 60 (△), 90 (+), 120 (×), 150 (◇), and 180° (▽). (b) Scattering phase $\theta(\beta,k)$ in radian vs. photoelectron wave vector k in Å^{-1} for oxygen at different scattering angles β where β = 0 (□), 30 (○), 60 (△), 90 (+), 120 (×), 150 (◇), and 180° (▽).

where $\delta_l(k)$ is the phase shift with angular momentum l and $P_l(\cos\beta)$ is the Legendre polynomial.

Substituting $\delta_l(k) = \delta_l^R + i\delta_l^I$ [where δ_l^R and δ_l^I are real and imaginary parts of $\delta_l(k)$] in eq 23, we have

$$f(\beta,k) = \sum_{l=0}^{\infty}\left(\frac{2l+1}{2k}\right)[(\sin 2\delta_l^R)e^{-2\delta_l^I} + i(1 - (\cos 2\delta_l^R)e^{-2\delta_l^I})]P_l(\cos\beta) \quad (24)$$

$$f^R(\beta,k) = \sum_{l=0}^{\infty}\left(\frac{2l+1}{2k}\right)(\sin 2\delta_l^R)e^{-2\delta_l^I}P_l(\cos\beta) \quad (24a)$$

$$f^I(\beta,k) = \sum_{l=0}^{\infty}\left(\frac{2l+1}{2k}\right)[1 - (\cos 2\delta_l^R)e^{-2\delta_l^I}]P_l(\cos\beta) \quad (24b)$$

Combining eq 13 and 24, we obtain

$$F(\beta,k) = ([f^R(\beta,k)]^2 + [f^I(\beta,k)]^2)^{1/2} \quad (25)$$

$$\theta(\beta,k) = \tan^{-1}\left[\frac{f^I(\beta,k)}{f^R(\beta,k)}\right] \quad (26)$$

Using the electron-atom scattering theory originally developed by Lee and Beni,[10] we have calculated the series of $\delta_l(k)$ for various elements in the periodic table as scatterers. $F(\beta,k)$ and $\theta(\beta,k)$ are then calculated from these complex phase shifts via eq 24–26. The results for carbon and oxygen are tabulated in Tables I and II (supplementary material), respectively. Some representative curves for oxygen using Herman–Skillman wave functions are shown in Figure 3. Other details of calculations have been reportedly in the literature.[10,11]

$F(\beta,k)$ and $\theta(\beta,k)$. It is apparent from Figure 3a that the amplitude has its maximum at β = 0° and attenuates rapidly as β increases. The high k region, however, drops off much faster than the low k region. At $\beta \gtrsim 30°$, $F(\beta,k)$ is generally quite small ($\lesssim 1$) with some fine structure which changes as β varies. The complexity of the fine structure also seem to increase with increasing atomic number Z.

Figure 3b shows that as β increases, the scatterer phase increases, first slowly at low β then at a faster rate. At high β values ($\beta \gtrsim 30°$), complex structures tend to develop which is related to the sampling of the core levels of the scattering atoms and hence is Z dependent.

In Figure 4, we show the dependence of scattering amplitude $F(\beta,k)$ on β for a few representative k values for oxygen. For all k values, the amplitude attenuates rapidly from its maximum value at β = 0° to $F \lesssim 1$ at $\beta \gtrsim 30°$. At low k values ($k \lesssim 9$ Å^{-1} for these elements), the amplitude exhibits both maxima and minima. For example, at k = 3.78 Å^{-1}, $F(\beta,k)$ for oxygen reaches its minimum at $\beta \sim 100°$ and its maxima at $\beta \sim 0$ and 180°. The maxima correspond to β values where multiple-scattering effect is most important and vice versa. The number of these extrema increases with increasing atomic number Z (e.g., there are two minima and three maxima for sulfur), corresponding to the sampling of the increasing number of electronic shells in the scattering atom. At sufficiently large k values ($k \gtrsim 9$ Å^{-1} for these elements), on the other hand, these extrema vanish, resulting in monotonically decreasing amplitude functions.

$\Omega(\beta,k)$ and $\omega(\beta,k)$. In this section, we shall illustrate the effect of the amplitude and phase modification factors, $\Omega(\beta,k)$ and $\omega(\beta,k)$, as a function of the scattering angle β, using oxygen as an example. For clarity, we set $e^{-\Delta r/\lambda} = 1$ in eq 21 and 22. We further assume r_{AB} = 1.95 Å and r_{BC} = 1.28 Å and calculate r_{AC}

(13) A. Messiah, "Quantum Mechanics", vol. I, Wiley, New York, 1970, p 386.

(14) Similar conclusion can be reached by comparing the scattering amplitude for copper calculated by using various approximations.[9]

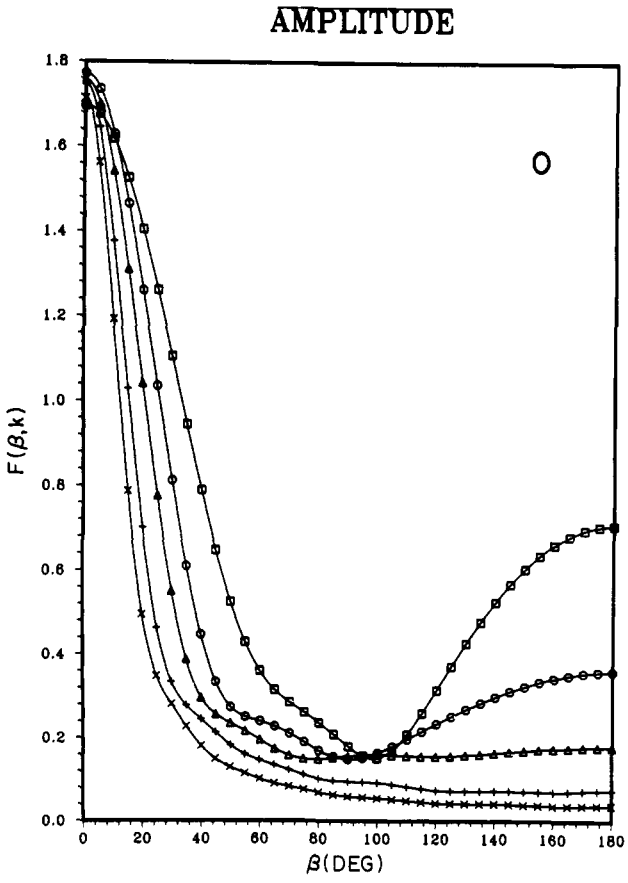

Figure 4. Scattering amplitude $F(\beta,k)$ (Å) vs. scattering angle β (deg) for oxygen at different k values where k = 3.7795 (□), 5.6692 (○), 7.5589 (△), 11.3384 (+), and 15.1178 (X) Å^{-1}.

from r_{AB}, r_{BC}, and β (cf. eq 15–17).

Figures 5 and 6 show the results for $\Omega(\beta,k)$ and $\omega(\beta,k)$, respectively, for β = 0–70°. It is immediately obvious that multiple scattering can lead to not only amplitude enhancement ($\Omega > 1$) but also amplitude reduction ($\Omega < 1$). At $\beta \sim 0°$, $\Omega(\beta,k)$ has the maximum magnitude [$\Omega(\beta,k) \sim 9$] and is generally a flat function of k. As β increases, $\Omega(\beta,k)$ attenuates rapidly, especially at high k region, reflecting the same functional feature of $F(\beta,k)$. At $\beta \sim 30°$, for example, $\Omega(\beta,k)$ drops to ~2.5 (amplitude enhancement) at low k values and ~0.4 (amplitude reduction) at high k values. At $\beta \sim 35°$, we observe an amplitude modification factor of 1.4, 0.37, and 0.65 for k ~4, 8, and 15 Å^{-1}, respectively. For even higher values of β, we find that $\Omega(\beta,k)$ exhibits characteristic features in k space for each β value, with its maxima and minima progressing smoothly as β changes. For example, at β = 50, 60, and 70°, $\Omega(\beta,k)$ reaches its peak values of 1.4, 1.5, and 1.6 at $k \sim$ 12, 7, and 5 Å^{-1}, respectively. Similarly, the minimum of $\Omega(\beta,k)$ of 0.82, 0.78, and 0.74 for $\beta \sim$ 60, 65, and 70° occurs at $k \sim$ 15.7, 13.2, and 10.7 Å^{-1}. The systematic progression of these extrema as β changes stems from the composite effect of $F(\beta,k)$ and $k(\Delta r)$ as they vary systematically with β. As we will soon see, the former factor is more important at low β values ($\beta \lesssim 30°$), whereas the latter dominates at high β values.

In contrast, the β dependence of the phase modification factor $\omega(\beta,k)$ is less dramatic as is evident from Figure 6. At $\beta \lesssim 20°$, the slope of ~−0.05 rad/Å^{-1} implies a distance correction of ~0.03 Å due to multiple scattering (involving oxygen at the distances assumed). At $\beta \sim 30°$ where the strongest β dependence is observed, the maximum slope of ~−0.20 rad/Å^{-1} will give rise to a distance correction of ~0.10 Å. For $\beta \gtrsim 50°$, $\omega(\beta,k)$ is once again a weak function of both β and k. For example, at $\beta \sim 55°$, a slope of ~0.10 rad/Å^{-1} will cause a correction in distance of ~−0.05 Å. It should be noted that these phase shift corrections are in general smaller than that caused by the corresponding backscatterer phase shift (β = 180°; cf. Figures 3b) and much smaller than those caused by central atom phase shifts.

In an attempt to understand the focusing (multiple scattering) effect in EXAFS, we plot in Figures 7 and 8 various components of $\Omega(\beta,k)$ and $\omega(\beta,k)$ for β = 0, 30, and 60° (at distances r_{AB} = 1.95 and r_{BC} = 1.28 Å). In Figures 7a–c, curves II and III represent the contributions $2\tilde{r}F(\beta,k)\cos\tilde{\theta}(\beta,k)$ and $[\tilde{r}F(\beta,k)]^2$, respectively, due to, approximately, the multiple scattering pathways II and III shown in Figure 2. The factor of $\cos\tilde{\theta}(\beta,k)$ in curve II arises from the cross term in phase. Simple sum of these two terms and the constant 1 (due to direct backscattering pathway I in Figure 2) gives $\Omega(\beta,k)$ (cf. eq 21). It is apparent that at low scattering angles ($\beta < 30°$), the relative importance of the three scattering pathways follows the order III > II > I. That is, multiple scattering via the intermediary atom B on both forward and returning trips is the dominant scattering process such that the functional form (shape) of the amplitude modification function $\Omega(\beta,k)$ resembles that of $[\tilde{r}F(\beta,k)]^2$. This is the origin of the focusing effect. In fact, strictly speaking, at $\beta \equiv 0°$, only this term (pathway III) needs to be considered. At higher β values ($\beta \gtrsim 60°$), the relative magnitude of the three scattering pathways follows the order I > II > III. That is, at high scattering angles, direct backscattering (pathway I) and the "round-the-triangle" multiple scattering (pathway II) are the most important scattering processes with the latter attenuating further as β increases. The shape (functional dependence on k) of the amplitude modification, $\Omega(\beta,k)$, is now determined mainly by that of $2\tilde{r}F(\beta,k)\cos\tilde{\theta}$ (i.e., curve II), since pathway I gives rise to only a constant 1 in eq 21. Within the term $2\tilde{r}F(\beta,k)\cos\tilde{\theta}(\beta,k)$ where $\tilde{\theta}(\beta,k) \simeq \theta(\beta,k) + k(\Delta r)$, the factor $k(\Delta r)$ is of most importance, since $\theta(\beta,k)$ is a rather weak function of k and β. This is the "phase" component in the amplitude modification factor. For high Z scatterers with a strong $F(\beta,k)$ function, $F(\beta,k)$ may also play an important role in determining $\Omega(\beta,k)$. Even at scattering angles as high as 90–120°, we can still find amplitude modification of ca. ±25% at low k regions due to multiple scattering. Hence amplitude transferability must be treated with caution.

In Figures 8a–c, we show the functions $\tilde{\theta}(\beta,k)$, $[rF(\beta,k)]^{-1}$, and $\omega(\beta,k)$ for β = 0, 30, and 60°, respectively [note that eq 22 can be rewritten as $\omega = 2\tan^{-1}(\sin\tilde{\theta}/[(\tilde{r}F)^{-1} + \cos\tilde{\theta}])$ for our purpose]. At low scattering angles ($\beta \lesssim 20°$), $[\tilde{r}F(\beta,k)]^{-1}$ is small since $F(\beta,k)$ is large, it is not surprising to find $\omega(\beta,k)$ resembling $\tilde{\theta}(\beta,k)$ in shape which, in turn, is similar to $\theta(\beta,k)$ since Δr is quite small (at $\beta \equiv 0°$, $\Delta r = 0$, $\tilde{\theta} \equiv \theta$). Hence, $\omega(\beta,k)$, like $\theta(\beta,k)$, is a weak function of both β and k. At high scattering angles ($\beta \gtrsim 50°$), on the other hand, $F(\beta,k)$ is small and Δr is large; $\omega(\beta,k)$ is therefore dominated by terms such as $\sin\tilde{\theta}$ and $[\tilde{r}F(\beta,k)]^{-1}$. Since $\sin\tilde{\theta} \lesssim 1$ and $[\tilde{r}F(\beta,k)]^{-1}$ is >> 1, we find a relatively small $\omega(\beta,k)$ which also has a weak k dependence. At the intermediate β angles, $\omega(\beta,k)$ has the strongest β and k dependence, since neither term in the denominator of eq 22 dominates (vide supra).

To summarize, we find that the amplitude enhancement at low scattering angles (focusing effect) stems mainly from the multiple-scattering process involving the intermediary atom in both the forward and the returning trip (pathway III in Figure 2), whereas the amplitude modification (enhancement and/or attenuation) at higher scattering angles, where both the direct backscattering (pathway I) and the round-the-triangle multiple scattering (pathway II) are important, comes from mainly the later multiple scattering process. While focusing effect can, at low scattering angles (large bond angles), cause an order of magnitude enhancement in amplitude, its impact on the phase is, fortunately, less dramatic. From our examples, we see that the corrections in distance determination due to multiple-scattering processes involving low Z intermediary atoms amount to less than ~0.10 Å.

Angle Determination

In this section, we shall describe a general method for interatomic angle determination by EXAFS on unoriented (spherically averaged) materials based on the theory and calculations described in the previous sections.

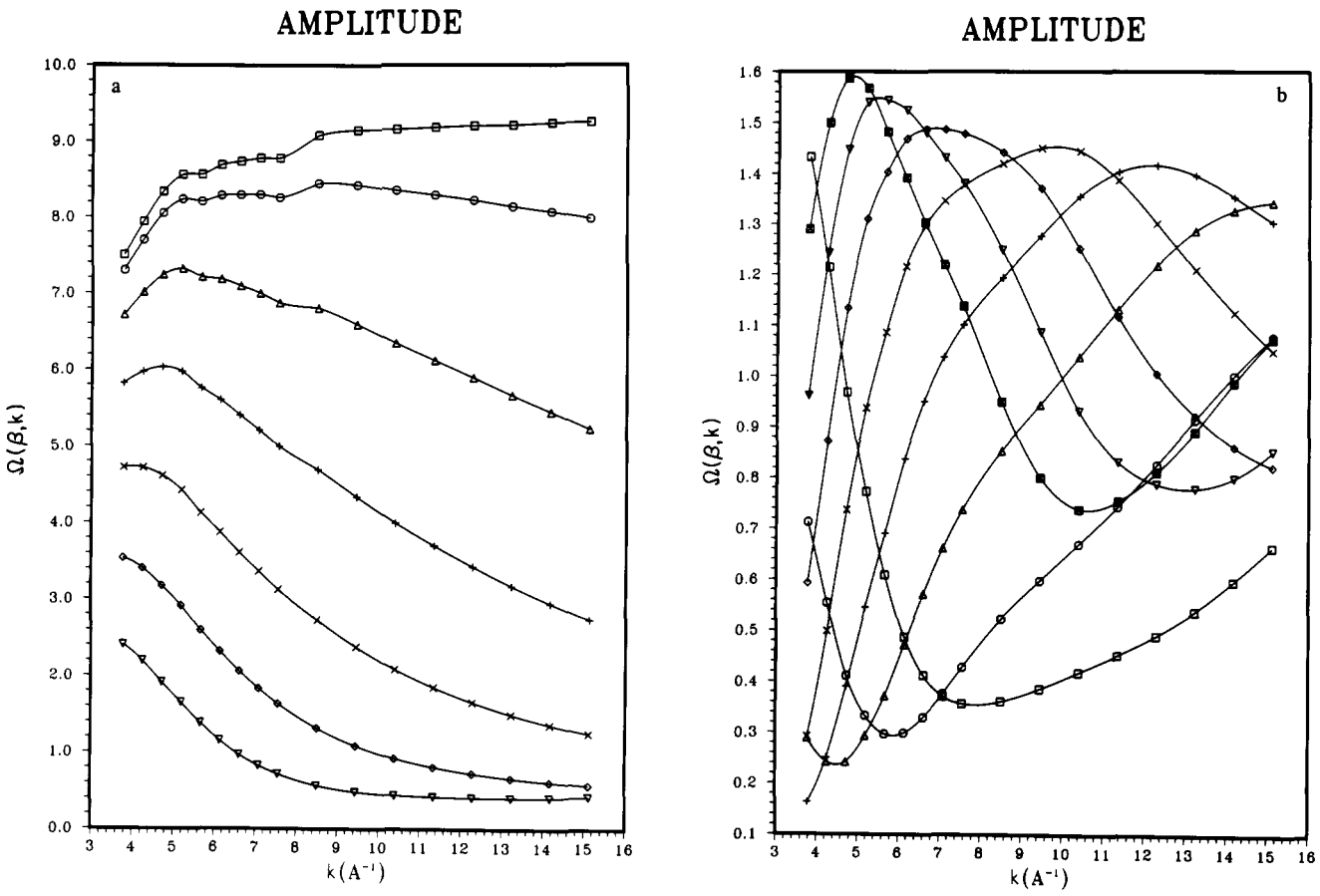

Figure 5. Amplitude modification factor $\Omega(\beta,k)$ vs. photoelectron wave vector k in Å^{-1} for oxygen with r_{AB} = 1.95 and r_{BC} = 1.28 Å as a function of scattering angle β where β = 0 (□), 5 (○), 10 (△), 15 (+), 20 (X), 25 (◇), and 30° (▽) for (a) and β = 35 (□), 40 (○), 45 (△), 50 (+), 55 (X), 60 (◇), 65 (▽), and 70° (⊠) for (b).

We will illustrate the usefulness, and the accuracy, of this method by three examples: (1) the virtually linear metal carbonyl Fe–C–O in $Na_2Fe(CO)_4$ (**1**), (2) the bent Pt–O–C in $K_2Pt(C_2O_4)_2$ (**2**), and (3) the bent Pt–O–S in $K_2Pt_2(SO_4)_4(H_2O)_2$ (**3**). The known bond angles of each of these three A–B–C systems are 177,[15a] 113,[16] and 124°.[17] Our goal is to determine enough structural parameters to completely characterize the triangle ABC.

Basically, the method involves four major steps: (1) data reduction to convert the $\mu(E)$ vs. E data to $\chi(k)$ vs. k data, (2) Fourier filtering of the EXAFS spectra $\chi(k)$ into two components, χ^{AB}(k) and χ^{AC}(k) corresponding to the A–B and the A–C distances, respectively, (3) curve fitting of $\chi^{AB}(k)$ (hereafter referred to as AB fit) to obtain structural information for the A–B bond, and (4) curve fitting of the $\chi^{AC}(k)$ (hereafter described as ABC fit) to obtain structural information involving the A–C distance and A–B–C angle.

Collection and Reduction of Data

The X-ray absorption measurements were performed at Stanford Synchrotron Radiation Laboratory (SSRL) by using the synchrotron radiation from Stanford Positron Electron Accelerating Ring (SPEAR) at Stanford Linear Accelerator Center (SLAC). The raw data were collected in the transmission mode by using the EXAFS I spectrometer. Details of the experiments can be found in our previous publications.[18-20]

Iron K edge, platinum L_I edge, and platinum L_{III} edge were measured for **1**, **2**, and **3**, respectively. The photon energy E was converted into photoelectron wave vector k by using eq 2 with the experimental threshold energy E_0^{exptl} of 7160, 13 920, and 11 565 eV for the Fe K, Pt L_I, and Pt L_{III} edge, respectively. After conversion to k space, the data were multiplied by k^3 and the background was removed by using a cubic spline technique containing three sections for iron and four sections for platinum. The data were then divided by the edge jump and corrected for the μ_0 dropoff via Victoreen's true absorption $\mu_0/\rho = C\lambda^3 - D\lambda^4$ equation with C = 126, 470, and 78.7 and D = 27.2, 219, and 15.6 for Fe K, Pt L_I, and Pt L_{III} edge, respectively.

Fourier Filtering

In order to separate the $\chi(k)$ into the two major components, $\chi^{AB}(k)$ and $\chi^{AC}(k)$, it is necessary to perform a Fourier filtering (vide supra) on the data. The Fourier transforms $\rho_3(r')$ of the $k^3\chi(k)$ EXAFS data are shown in Figures 9a–c for the three compounds. It is apparent that for **1** and **2**, the radial distribution function (RDF) contains two distinct peaks: the shorter distance corresponds to the first coordination shell (viz., A–B distances) while the longer distance corresponds to the second shell (viz., A–C distances). For **3**, the RDF shows three peaks corresponding to (in increasing distance) Pt–O, Pt–Pt, and Pt···S backscatterings. The A–C peak in **1** has a magnitude greatly enhanced by focusing effect (suggesting a Fe–C–O moiety close to linearity) in contrast to the much weaker peaks in **2** and **3** (expected from the single-scattering theory for bond angles of ~120°). The dashed curves in Figure 9 are the smooth filtering functions used to isolate

(15) (a) R. G. Teller, R. G. Finke, J. P. Collman, H. B. Chin, and R. Bau, *J. Am. Chem. Soc.*, **99**, 1104 (1977); (b) H. B. Chin and R. Bau, *ibid.*, **98**, 2434 (1976).
(16) V. R. Mattes and K. Krogmann, *Z. Anorg. Allg. Chem.*, **332**, 247 (1964).
(17) G. S. Muraveiskaya, G. A. Kukina, V. S. Orlova, O. N. Evstafêva, and M. A. Porai-Koshits, *Dokl. Akad. Nauk SSSR*, **226**, 596 (1976).
(18) B. K. Teo, P. Eisenberger, and B. M. Kincaid, *J. Am. Chem. Soc.*, **100**, 1735 (1978).
(19) B. K. Teo, R. G. Shulman, G. S. Brown, and A. E. Meixner, *J. Am. Chem. Soc.*, **101**, 5624 (1979).
(20) (a) B. K. Teo, K. Kijima, and R. Bau. *J. Am. Chem. Soc.*, **100**, 621 (1978); (b) B. K. Teo, P. Eisenberger, J. Reed, J. K. Barton, S. J. Lippard, *ibid.*, 100, 3225 (1978).

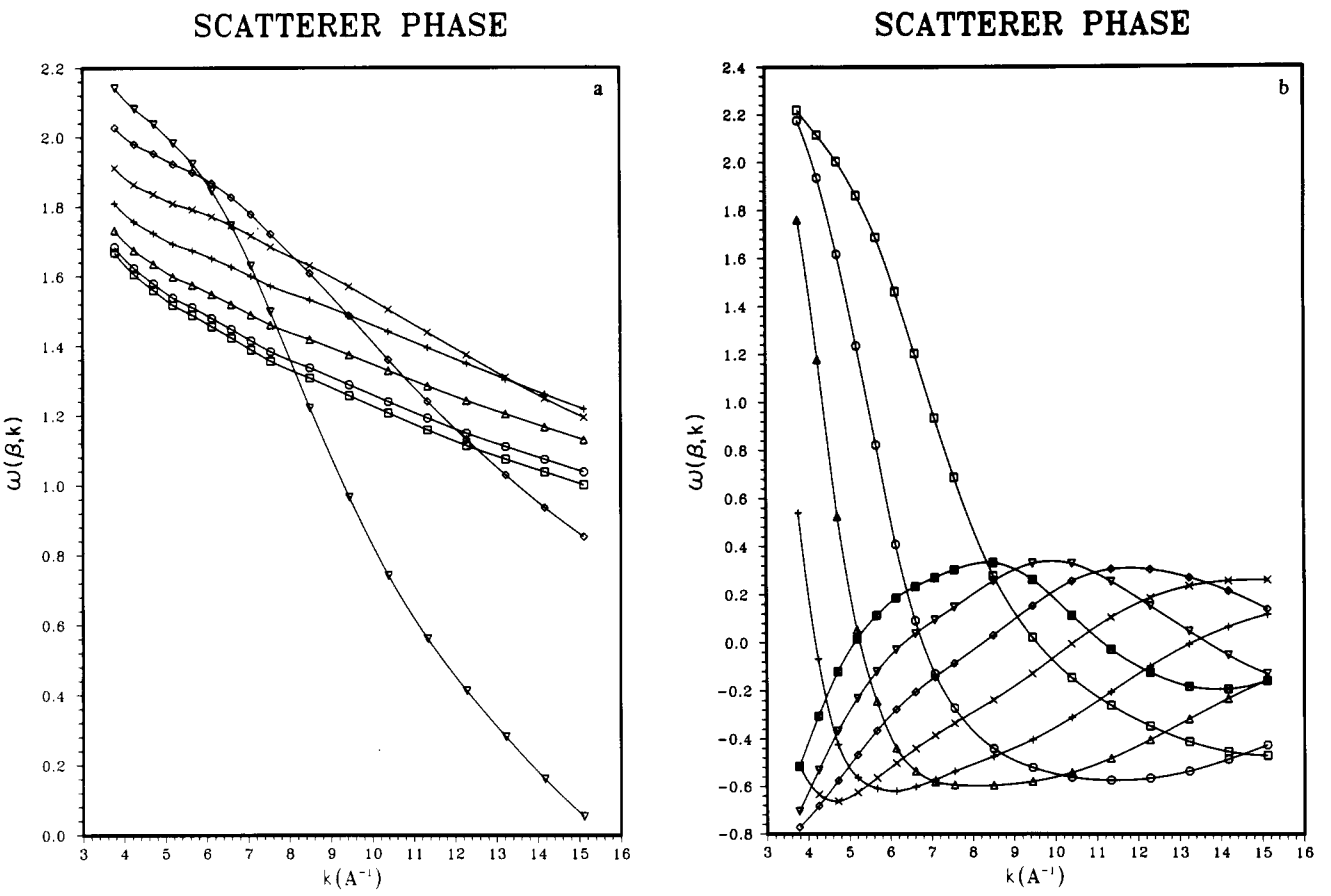

Figure 6. Phase modification factor $\omega(\beta,k)$ in radian vs. photoelectron wave vector k in Å^{-1} for oxygen with r_{AB} = 1.95 and r_{BC} = 1.28 Å as a function of scattering angle β where β = 0 (□), 5 (○), 10 (△), 15 (+), 20 (X), 25 (◇), and 30° (▽) for (a) and β = 35 (□), 40 (○), 45 (△), 50 (+), 55 (X), 60 (◇), 65 (▽), and 70° (⊠) for (b).

the A–B and A–C distances. Back transforming these two contributions to k space gives rise to $\chi^{AB}(k)$ and $\chi^{AC}(k)$ which were used for the following curve fittings.

AB Fits. The first-shell contribution $\chi^{AB}(k)$ can be fitted with the following model based on eq 4:

$$k^3\chi^{AB}(k) = S_B N_B F_B(k_B) k_B^2 e^{-2\sigma_B^2 k_B^2} e^{-2\eta_B r_{AB}/k_B^n} \left(\frac{\sin [2k_B r_{AB} + \phi_{AB}(k_B)]}{r_{AB}^2} \right) \quad (27)$$

where the subscripts B and AB refer to atom B and the A–B bond, respectively (A is the absorber and B is the backscatterer). Here we use the theoretical amplitude, $F_B(k) \equiv F_B(\pi,k)$, and phase shifts, $\phi_{AB}(k) = \phi_A(k) + \phi_B(k) - l\pi$ (where l = 1 for K and L_I edges and l = 0 for L_{III} edge), without parametrization. Since the phase functions are unique only when a particular energy threshold E_0 is specified, our choice of E_0^{exptl} may not be consistent with the theoretical E_0's for each of the different types of neighbors for which the theoretical phase shifts are calculated. We must therefore allow a different E_0 value in eq 2 for each type of neighboring atom. We define

$$\Delta E_{0_j} = E_{0_j}^{th} - E_0^{exptl} \quad (28)$$

$$k_j = (k^2 - 2(\Delta E_{0_j})/7.62)^{1/2} \quad (29)$$

where k is the "experimental" wave vector with experimental threshold energy E_0^{exptl} and k_j is the "theoretical" wave vector with the theoretical threshold energy $E_{0_j}^{th}$ associated with atom j. The parameter ΔE_{0_j} is refined in the curve fitting. For AB fits, j stands for atom B.

In eq 27 we approximated the electron inelastic mean free path with

$$\lambda_j(k) = k^n/\eta_j \quad (30)$$

where n = 1 or 2 can be used, so long as the same n is used throughout the entire data analysis (our experience showed that the best fits occur at $1 < n < 2$). A better model for $\lambda(k)$ will be

$$\lambda(k) = 1/\eta[k^n + (\xi/k)^4] \quad (31)$$

since it has been shown by Powell,[21] Penn,[22] Seah and Dench[23] that $\lambda(E) \propto E$ at high energies ($E \gtrsim 500$ eV), $\propto E^{1/2}$ at intermediate energies ($100 \lesssim E \lesssim 500$ eV), and $\propto E^{-2}$ at low energies ($E \lesssim 50$ eV). We found, however, for EXAFS data with $k \gtrsim 5$ Å^{-1}, eq 30 is adequate. Though both n = 1 and n = 2 models can give rise to about the same quality fit for our data, it should be pointed out that the latter generally yields values of λ in the range 2–14 Å (for k = 5–13 Å^{-1}), more in line with that predicted by the universal curves for electron inelastic mean free paths.[21-23] If EXAFS data with $k \lesssim 5$ Å^{-1} are included, eq 31 gives a better fit in the low k region. In our case, since theoretical amplitude and phase functions are less reliable for $k \lesssim 4$ Å^{-1}, we truncate all the filtered data at $k \sim$ 5–13 Å^{-1} and use eq 30 for the curve fittings.

In eq 27 we also included an overall scale factor S in order to best fit the EXAFS spectra with the theoretical functions. Strictly speaking, one should include an amplitude reduction factor $s_0^2(k) \lesssim 1$, which is a function of k, to account for the many body effects ("shake-up" and "shake-off" processes in which one or more passive electrons are excited along with the photoelectron) at the central atom.[24] In general, $s_0^2(k) \sim 1$ at low k values and $s_0^2(k)$

(21) C. J. Powell, *Surf. Sci.*, **44**, 29 (1974).
(22) D. R. Penn, *Phys. Rev. B*, **13**, 5248 (1976).
(23) M. P. Seah and W. A. Dench, *Surf. Inter. Anal.*, **1**, 2 (1979).
(24) E. A. Stern, B. A. Bunker, and S. M. Heald, *Phys. Rev. B*, **21**, 5521 (1980).

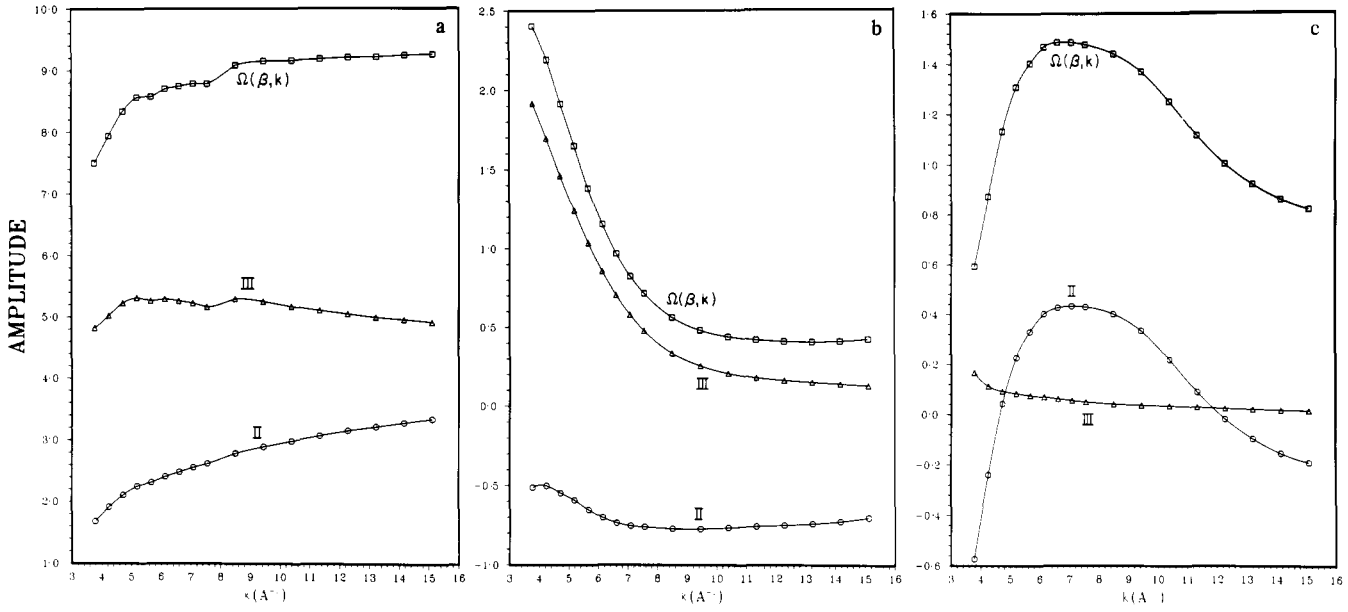

Figure 7. Multiple-scattering contributions to the amplitude modification factor $\Omega(\beta,k)$ (□) vs. k in Å^{-1} due to pathways II (△) and III (○) in Figure 2 for oxygen at different scattering angles β where β = 0 (a), 30 (b), and 60° (c). Curves II and III correspond to the functions $2\tilde{r}F(\beta,k)\cos\tilde{\theta}(\beta,k)$ and $[\tilde{r}F(\beta,k)]^2$, respectively, defined in the text.

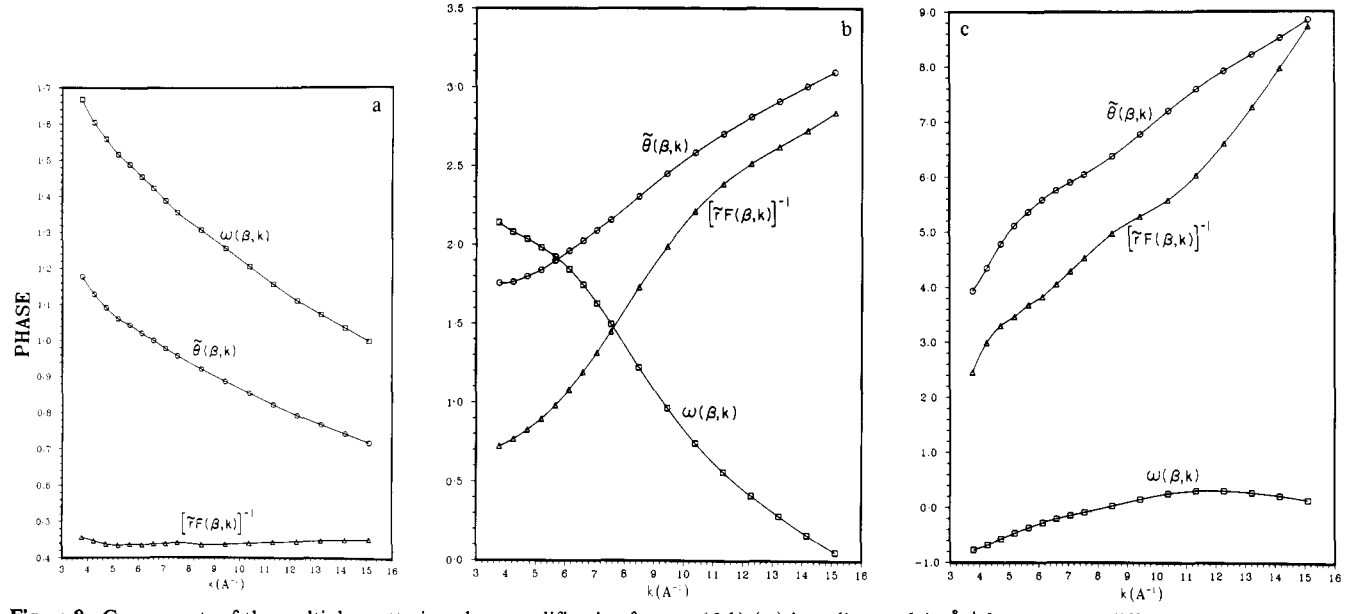

Figure 8. Components of the multiple-scattering phase modification factor $\omega(\beta,k)$ (□) in radian vs. k in Å^{-1} for oxygen at different scattering angles β where β = 0 (a), 30 (b), and 60° (c). The curves are $\tilde{\theta}(\beta,k)$ (○) and $[\tilde{r}F(\beta,k)]^{-1}$ (△) defined in the text.

$\sim$ 0.6–0.8 for $k \gtrsim 7$ Å^{-1}. For our purpose, we chose to use the overall scale factor S as a parameter to facilitate best fitting of the data and compensate for the breakdown, if any, of the amplitude transferability. Thus, S is meaningful only when comparing chemically and structurally similar systems with similar σ and η values.

For each $\chi^{AB}(k)$ fit, five parameters are least squares refined: the overall scale factor S, the Debye–Waller factor σ_B, the mean free path parameter η_B, the distance r_{AB}, and the threshold energy difference ΔE_{0_B}. The results are listed in Table III (supplementary material) and the best fits (for n = 1) are depicted in Figure A, a–c (supplementary material), as dashed curves. The least-squares fitted r_{AB} distances of 1.77 (3), 2.03 (2), and 1.95 (3) Å for compound 1–3, respectively, agree quite well with the corresponding known distances of 1.75 (1) Å [Fe–C in $K_2Fe(CO)_4$],[15a] 2.00 (1) Å [Pt–O in $K_2Pt(C_2O_4)_2\cdot 2H_2O$)],[16] and 1.98 Å [Pt–O in $K_2Pt_2(SO_4)_4(H_2O)_2$].[17]

ABC Fits. In order to determine the A–B–C angle, the $\chi^{AC}(k)$ EXAFS contribution must be analyzed with the following model, which takes into account not only direct backscattering from atom C but also multiple scatterings via the intermediary atom B:

$$k^3\chi^{AC}(k) = S_C N_C \Omega_B(\beta,k_B) F_C(k_C) k_C^2 e^{-2\sigma_C^2 k_C^2} e^{-2\eta_C r_{AC}/k_C^n} \times \left(\frac{\sin(2k_C r_{AC} + \phi_{AC}(k_C) + \omega_B(\beta,k_B))}{r_{AC}^2} \right) \quad (32)$$

This model is based on eq 20–22 with k_B and k_C given by eq 29. The scattering amplitude functions $F_C(k) \equiv F_C(\pi,k)$ and $F_B(\beta,k)$ and the scattering phase functions $\phi_C(k) \equiv \theta_C(\pi,k)$ and $\phi_B(\beta,k)$ were taken from Tables I and II (supplementary material).[25] The

(25) The backscattering amplitude $F(k)$ and phase $\phi_b(k)$ functions for sulfur using Herman–Skillman wave functions are 0.7942, 0.7944, 0.7388, 0.6408, 0.5735, 0.5377, 0.5011, 0.4472, 0.3906, 0.3258, 0.2608, 0.2156, 0.1734, 0.1462, 0.1199, 0.1024, 0.0862 and 3.4496, 3.3513, 3.2724, 3.1725, 3.0328, 2.8831, 2.7528, 2.6413, 2.5212, 2.2951, 2.0464, 1.8424, 1.6261, 1.4096, 1.2219, 1.0176, 0.8610, respectively, at k = 3.7795, 4.2519, 4.7243, 5.1967, 5.6692, 6.1416, 6.6140, 7.0865, 7.5589, 8.5038, 9.4486, 10.3935, 11.3384, 12.2832, 13.2281, 14.1729, 15.1178.

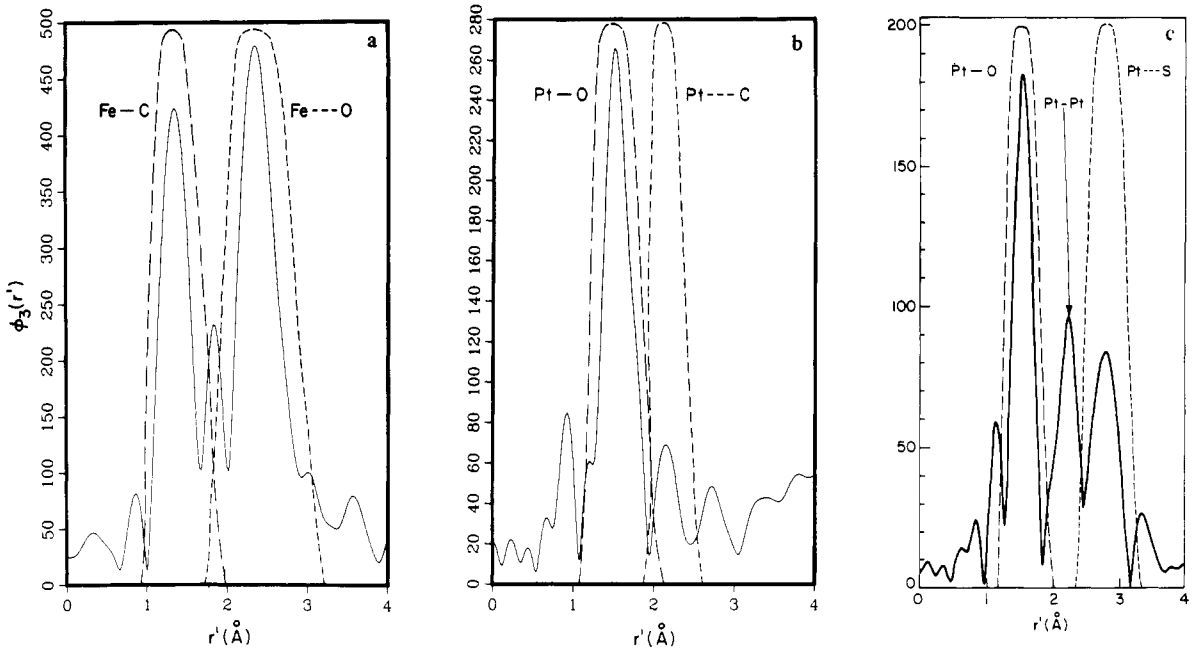

Figure 9. Fourier transforms (solid curves) and the filtering windows (dashed curves) of the $k^3\chi(k)$ vs. k data for (a) $Na_2Fe(CO)_4$ (Fe K edge), (b) $K_2Pt(C_2O_4)_2$ (Pt L_I edge), and (c) $K_2Pt_2(SO_4)_4(H_2O)_2$ (Pt L_{III} edge).

central atom phase functions $\phi_a^{\ l} = {}^1(k)$ were taken from Teo and Lee (Table VII for **1** and **2** and VIII for **3**).[11] To determine the bond angle A–B–C (=180 − β), the distance r_{AC}, and the Debye–Waller factor σ_C, we simply attempt to best fit the experimental curve with eq 32 by least-squares refining β, r_{AC}, σ_C, ΔE_{0_C}, η_C, and S_C. The distance r_{AB} and the energy correction ΔE_{0_B} were taken from the AB fit and held constant throughout the curve fitting process. The distance r_{BC} was calculated from r_{AB}, r_{BC}, and β in each cycle of refinement. The best fits are shown in Figure 10, while the resulting parameters are summarized in Table IV (supplementary material).

Figure 11a–c shows the Chi-square (Σ^2) plots for the angle A–B–C. The minimum (best fit) occurs at β = 0, 70, and 58 for **1**, **2**, and **3**, respectively, for either n = 1 (curve a) or n = 2 (curve c). Since the results are insensitive to n for **1** and **2** (except the expected changes in η, σ, and S), we chose to use n = 1 for **3**. If we restrict η_C = 0 (i.e., assuming $e^{-2r_{AC}/\lambda} = 1$ we find in general much worse fits with the Σ^2 minima shifted to lower β values (curve b in Figure 11). For example, the best fit (Σ^2 minimum) in **2** and **3** changes from β = 70 to β = 62° and β = 58 to β = 45°, with the quality of fit worse by three- and tenfold, respectively. For **1**, the fit with η_C = 0 is so unsatisfactory that the Σ^2 increases by over 40-fold, though the minimum remains at β = 0. The reason is that the amplitude envelope with η_C = 0 is inadequate at low k values. Our experience shows that fitting parameters related to the electron mean free path (such as η_C) are particularly crucial in fitting the *low k* amplitude for *low Z* scatterers and/or low β angles, since theory predicts a monotomically decreasing scattering amplitude in such cases.

We note that the fitting model with freely varying η_C is the most liberal approach within the context of eq 32 and therefore will give rise to the shallowest minimum. Any restriction on η_C and/or σ_C and/or r_{BC} will undoubtedly produce sharper Σ^2 minima which must lie within the boundary of curve a in Figure 11 and at higher Σ^2 (i.e., worse fits).

The kinks in the Σ^2 minima observed for **3** (cf. Figure 11c) deserve some comments. We believe that these kinks are caused by the interplay between the two highly correlated parameters η_C and σ_C. Figure Ba–c (supplementary material) depicts the variation of η_C and σ_C (least squares refined) for **1**–**3**, respectively, as a function of β. The two parameters correlate intimately to best fit the experimental amplitude. Such a correlation will produce a smooth Σ^2 vs. β plot if both parameters have ample range to vary as in **1** or **2**. This is not the case for **3** where σ_C drops to zero for β between 55 and 60°. Since σ cannot become negative in our model, these discontinuities in the multiparameter space may have caused the kink in the Σ^2 vs. β plot.

Table V. Comparison of Mean Structural Parameters from EXAFS Spectroscopy and X-Ray Crystallography for $Fe(CO)_4^{2-}$ (**1**), $Pt(C_2O_4)_2^{2-}$ (**2**), and $Pt_2(SO_4)_4(H_2O)_2^{2-}$ (**3**)[a]

compd	parameter	EXAFS[b]	crystallography	error, %
1	Fe-C[c]	1.77 (3)[f]	1.746 (4)[g]	+2
	C-O[d]	1.02 (7)	1.175 (5)[g]	−13
	Fe···O[d]	2.79 (1)	2.920 (–)[h]	−4
	Fe-C-O[d]	180 (21)	176.6 (3)[i]	+2
	Fe-C-O[e]	180 (15)	176.6 (3)[i]	+2
2	Pt-O[c]	2.03 (2)	2.00 (1)[j]	+2
	O-C[d]	1.07 (14)	1.29 (3)[j]	−17
	Pt···C[d]	2.60 (2)	2.77 (–)[h]	−6
	Pt-O-C[d]	110 (4)	113 (1)[k]	−3
	Pt-O-C[e]	118 (13)	113 (1)[k]	+4
3	Pt-O[c]	1.95 (3)	1.98 (–)[l]	−1
	O-S[d]	1.59 (8)	1.55 (–)[l]	+3
	Pt···S[d]	3.11 (1)	3.13 (–)[h]	−1
	Pt-O-S[d]	122 (4)	124 (–)[m]	−2
	Pt-O-S[e]	135 (7)	124 (–)[m]	+9

[a] Interatomic distances (Å) and angles (deg) are designated as A–B and A–B–C, respectively, with esd's (in parentheses). [b] All EXAFS results are for n = 1. [c] From best AB fits. [d] From best ABC fits. [e] From best ABC fits with η_C = 0. [f] The fitting errors for each parameter (in parentheses) were obtained by changing that particular parameter, while least squares refining the other parameters (which are varied in the Σ^2 minimum search) until Σ^2 is doubled. [g] From $K_2Fe(CO)_4$.[15a] Average Fe–C and C–O distances for two independent $Fe(CO)_4^{2-}$ dianions in $Na_2Fe(CO)_4 \cdot 1.5(C_4H_8O_2)$[15b] are 1.742 (6) and 1.167 (8) Å, respectively. [h] Calculated from average A–B, B–C, and A–B–C. [i] The two crystallographically independent Fe–C–O angles in $Na_2Fe(CO)_4 \cdot 1.5(C_4H_8O_2)$[15b] are 178.7 (5) and 171.0 (4)°. The average Fe–C–O angle of 175° gives rise to Fe···O distance of 2.906 Å. [j] From $K_2Pt(C_2O_4)_2 \cdot 2H_2O$.[16] [k] Calculated from the reported O–Pt–O and O–C–C angles.[16] by assuming the 5-membered PtO_2C_2 ring of the $Pt(C_2O_4)_2^{2-}$ dianion to be planar. [l] From $K_2Pt_2(SO_4)_4(H_2O)_2$.[17] [m] Calculated from the reported Pt–Pt, Pt–O, and O–S distances [17] by assuming the Pt_2O_2S ring to be planar and O···O ≈ 2.53 Å (calculated from the assumed O–S–O of 109.5°).

Comparison of EXAFS and Crystallographic Results

Table V compares the mean structural parameters derived from EXAFS spectroscopy (this work) with those from X-ray diffraction

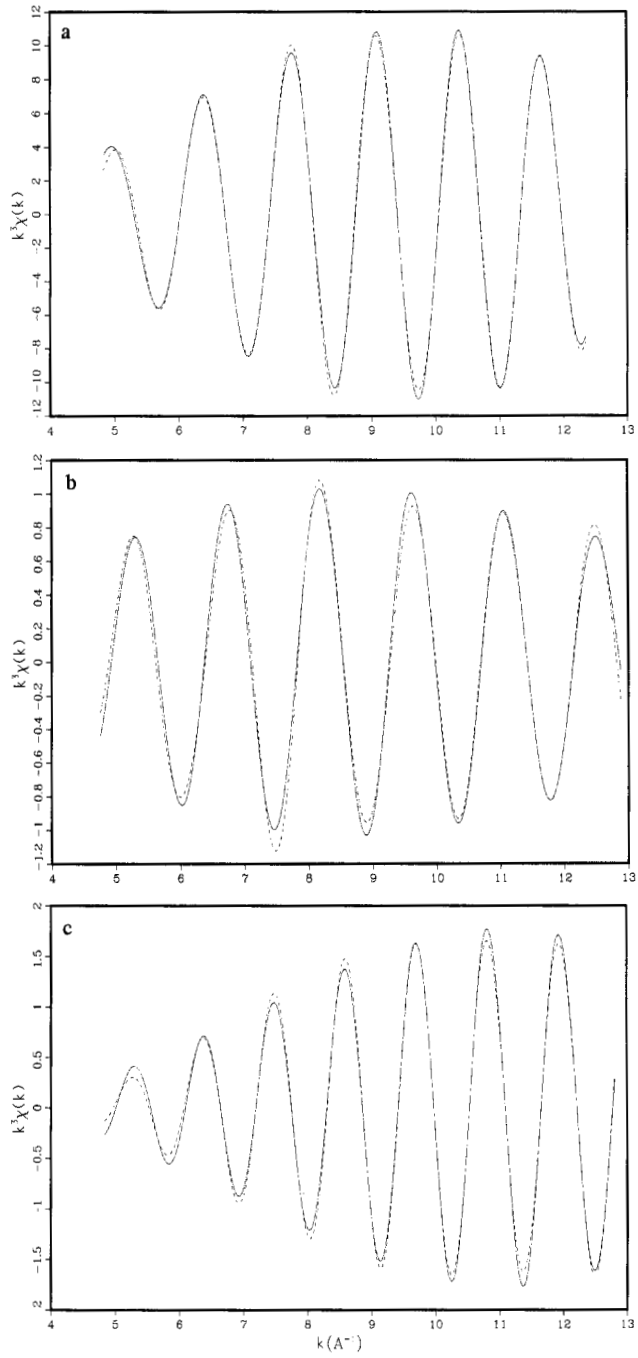

Figure 10. Fourier filtered EXAFS $k^3\chi^{AC}(k)$ vs. k spectra (solid curves) and the theoretical fits (dashed curves) for (a) $Na_2Fe(CO)_4$ where AC represents Fe···O, (b) $K_2Pt(C_2O_4)_2$ where AC represents Pt···C, and (c) $K_2Pt_2(SO_4)_4(H_2O)_2$ where AC represents Pt···S. See text for details of least-squares fits.

studies.[15-17] For **1** the distance Fe···O was calculated from the published Fe–C and C–O distances and the Fe–C–O angle.[15a] For **2**, the Pt–O–C angle was calculated from the reported O–Pt–O and O–C–C angles[16] by assuming the five-membered PtO_2C_2 ring of the $Pt(C_2O_4)_2^{2-}$ dianion to be planar. For **3**, the Pt–O–S angle was calculated from the reported Pt–Pt, Pt–O, and O–S distances[17] by assuming the five-membered Pt_2O_2S ring to be planar and an O···O contact of 1.53 Å (estimated from the assumed O–S–O angle of 109.5°). Finally, the A···C distance in **2** and **3** were calculated from the reported A–B and B–C distances and the calculated A–B–C angle.

It is apparent from Table V that EXAFS spectroscopy, with the multiple-scattering formulation presented here and the use of purely ab initio theoretical amplitude and phase functions, is capable of providing accurate interatomic distances and angles

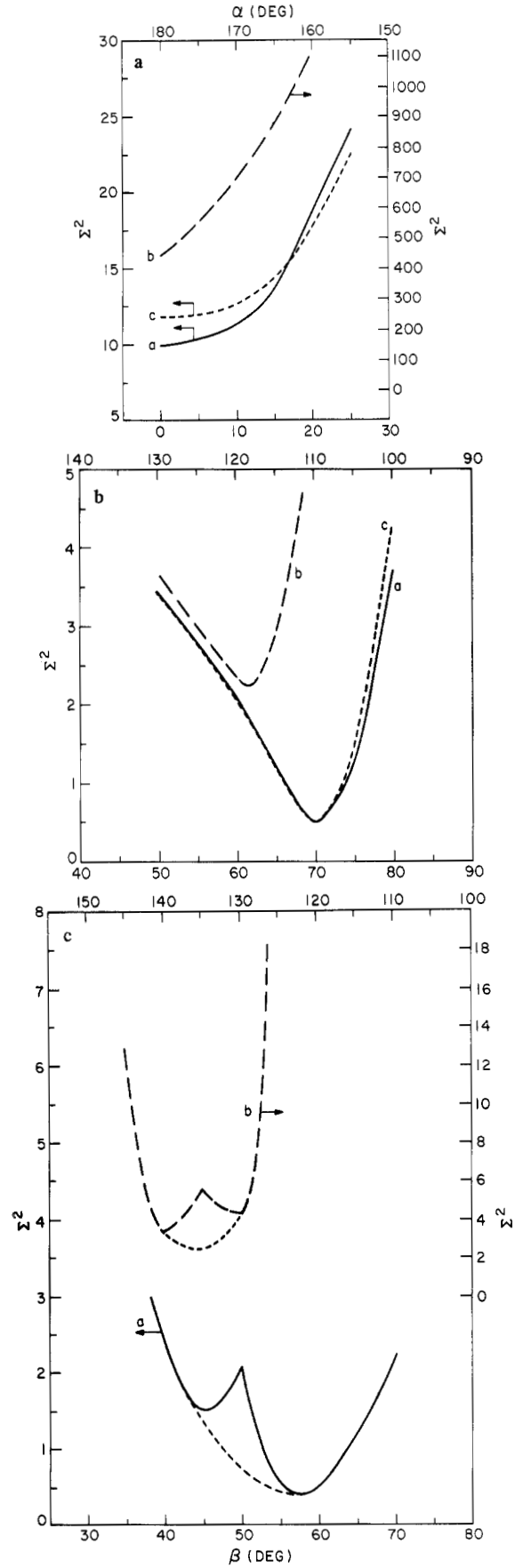

Figure 11. The chi squares Σ^2 (the sume of squares of the residuals) vs. the A–B–C bond angle α in degree (or the scattering angle $\beta = 180° - \alpha$) for the ABC fits of (a) $Na_2Fe(CO)_4$, (b) $K_2Pt(C_2O_4)_2$, and (c) $K_2Pt_2(SO)_4(H_2O)_2$. Curve a, least squares refining η_C for $n = 1$; curve b, holding $\eta_C = 0$; curve c, least squares refining η_C for $n = 2$. See text for other details of the fits.

on unoriented samples. For example, a comparison of the *first-shell* A–B distances from EXAFS with the corresponding diffraction values revealed an accuracy of better than 2%. A similar comparison of the *second-shell* A–C distances with the known values[15-17] (2.79 (1) vs. 2.92 (–) Å for **1**, 2.60 (2) vs. 2.77 (–) Å for **2**, and 3.11 (1) vs. 3.13 (–) Å for **3** revealed that the EXAFS results tend to be about ≤6% too low for low Z ($Z \leq 10$) scatterers but within 3% for high Z scatterers (again, generally too low). The cause of this shrinkage for higher shell distances, especially for low Z scatterers, is presently under investigation. It might be related to the well-known shrinkage in EXAFS distance for systems with asymmetric pair correlation functions or anharmonic vibrations. For **1–3**, the nonbonding nature of the A–C distances may have caused the shrinkage. As a result of the shrinkage in A–C, the indirectly determined B–C distances are in error by ca. ≤18%, mostly too low for low Z scatterers [1.02 (7) vs. 1.18 (1) Å for **1**, and 1.07 (14) vs. 1.29 (3) Å for **2**).[16] On the other hand, the better accuracies in determining the A–B (≤2%) and A–C (≤3%) distances and the A–B–C angle (≤3%) for high Z scatterers ($Z \leq 10$) give rise to an accuracy of ca. 3% in the B–C distance (1.59 (8) vs. 1.55 (–) Å for **3**).[17]

As evident from Table V, the accuracy for angle determination is better than 6% for low Z ($Z \leq 10$) and 3% for high Z scatterers, if η_C is allowed to vary (i.e., least squares refined). In most cases, it amounts to an accuracy of better than ca. 5°, which is comparable to the scattered range of crystallographically independent bond angles often observed in diffraction studies.

Since the B–C distance is determined indirectly from the A–B and A–C distances and the A–B–C angle, it is not surprising that it has the least accuracy. In the case of low Z scatterers, the error arises from the error in A–C determination. If the shrinkage of the A–C distance can be rectified theoretically or calibrated experimentally, the B–C distance can be calculated with a better accuracy.

Discussions

It is interesting to ponder why angle determination is feasible by EXAFS spectroscopy for unoriented samples (e.g., noncrystalline or polycrystalline materials). Even more puzzling is the question that at bond angles $\alpha \lesssim 120°$ where the focusing effect is virtually disappearing, such angular determination is still possible. If, as mentioned in previous sections, the phase correction factor ω due to multiple scatterings is normally quite small, it might be concluded that the well-defined Σ^2 minima observed for the angle must be related to the amplitude modification. This rationale is understandable for bond angle α approaching 180° ($\alpha \gtrsim 150°$) where both the magnitude and the shape of the scattering amplitude change dramatically with the angle. For $90 \lesssim \alpha \lesssim 120°$, the scattering amplitude changes only slightly. Yet the amplitude modification factor Ω exhibits characteristic shape for each α. The reason is that at these angles, Δr becomes large such that the second term $[k(\Delta r)]$ in $\tilde{\theta}(\beta,k)$ (cf. eq 17), which is now a strong function of k, becomes the dominant factor. It is therefore not surpising to find Ω (cf. Figure 5), as well as ω (cf. Figure 6), to be highly dependent upon (i.e., fast varying) the bond angle α. *As α deviates far from the correct value, in either direction (viz., beyond the correlation limits of other parameters such as ΔE_0), the wrong distances give rise to progressively worsening phase mismatch which causes the quality of the fit to deteriorate rapidly (thereby producing a well-defined Σ^2 minimum).*

We must also conclude from this work that multiple-scattering processes involving three atoms (including the absorber and two neighboring atoms: cf. Figures 1 and 2) are important in determining the EXAFS of the *distant* shells, especially at large bond angles α. Multiple scatterings involving more than three atoms are likely to be of less importance due to the large effective total path length $2r_{eff}$ (vide supra), except, perhaps, in cases where all the bond angles are close to linearity. Yet the single-scattering theory has so far been successful in providing accurate distance, but not angle, information because of two facts. First, the effect in distance due to multiple scatterings is no more than 0.1 Å; in fact, in most cases ($\alpha \gtrsim 130°$), less than ca 0.03 Å (cf. Figure 6). A large part of such phase effect can be compensated by varying ΔE_0. Second, the effect in amplitude due to multiple scatterings is generally less than ca. 70% for $\alpha \lesssim 150°$. The envelope of such amplitude effect (i.e., shape of Ω, cf. Figure 5b) is such that a large portion of which can be compensated by σ and λ. For $\alpha \gtrsim 150°$, the large amplitude enhancement Ω is accompanied by a relatively weak k dependence such that the effect can largely be compensated by the overall scale factor S. Therefore, in a sense, the single-scattering theory, which contains no angle information, corresponds to one section (with β fixed at the true value) of the present multiple-scattering formalism in which $\Omega(\beta,k)$ and $\omega(\beta,k)$ are rapidly varying (cf. Figures 5 and 6). The dependence of the multiple-scattering effects on β and k makes possible the accurate bond angle determination by EXAFS spectroscopy described in this paper.

It should also be cautioned that in Fourier filtering, one should not filter out the multiple scattering pathways II and III which correspond to effective distances of $(r_{AB} + r_{BC} + r_{AC})/2$ (II in Figure 2) and $(r_{AB} + r_{BC})$ (III in Figure 2), respectively, by choosing too narrow a window for the A–C peak. For our examples, these "multiple-scattering peaks" are buried under the A–C peak in the Fourier transform (except, perhaps, III in **2** which is much less important than II). For systems with large $(r_{AB} + r_{BC} - r_{AC})/2$, each of these peaks may need to be analyzed separately by using the corresponding term in eq 10. Fortunately, for most systems with large α, III > II > I and $r_{AB} + r_{BC} \sim r_{AC}$, whereas for most systems with small α, I > II > III and $(r_{AB} + r_{BC} + r_{AC})/2 \gtrsim r_{AC}$. That is, for both limits of α, the dominant term(s) is (are) more likely than not to be buried under (or lie close to) the A–C peak.

It is apparent from this work that one must have a set of good amplitude and phase functions for each scattering angle for the intermediary atom as well as a consistent set of backscattering amplitude and phase functions for the terminal atom (backscatterer). One must also combine structural information obtained from AB and ABC fits in a consistent way to uniquely define the triangle. Furthermore, if model compounds with closely related structures are known, analysis of their EXAFS spectra will allow scaling (if any) of the amplitude parameters as well as calibration (if any) of the phase factors. This would greatly improve the accuracy, since both theoretical and experimental inadequacies tend to cancel out.

Throughout this paper, we assume that the number and identity of the neighboring atoms are known. In cases where this is not true, we expect this method to be difficult, if not impossible, to implement merely because of the fact that strong correlations between various parameters and/or functions can occur. Nevertheless, this method is capable of differentiating significantly different atom types and/or atom counts in addition to determining the structural parameters (distances and angles).

Conclusion

In this paper, we have developed a new EXAFS formulation which takes into account the effect of multiple scatterings. We have performed theoretical calculations on the scattering amplitude and phase shift, both as a function of the scattering angle. Combining the new formulation and the new theoretical functions enable us to unravel the "focusing" effect as well as to assess the relative importance of various multiple scattering processes as the scattering angle varies. On this basis, a novel method for interatomic angle determinations by EXAFS is devised and applied to a few known systems to illustrate the usefulness and accuracy of the technique. Further refinement of the method described in this paper will undoubtedly give rise to more accurate structural parameters, including interatomic distances and angles. On the other hand, the ultimate accuracy of such structural determination will depend heavily on the quality of the EXAFS data, especially the amplitude.

Extensive application of the angle determination technique developed in this paper to a wide variety of systems is in progress. Examples include stereochemical information beyond the first coordination shell for inorganic and biological systems, especially

when the ligand atoms are arranged in a nearly collinear fashion, solution structural determinations such as those pertaining to the ligand fluxionality and kinetics, ligation of simple well-defined molecules to biological molecules in solution, etc. It is clear that such structural information involving the distant, normally nonbonding, shells can greatly facilitate either interpretation of the mode of binding of known ligands or identification of the unknown ligands. These applications will be subjects of future publications.

Acknowledgment. I am indebted to Dr. P. A. Lee (Bell Laboratories) for his generous assistance and consultations throughout the course of this work. I am also grateful to Dr. J. Rowe (Bell Laboratories) and Dr. C. J. Powell (NBS) for helpful discussions on electron mean free path. Thanks also go to Dr. B. M. Kincaid, A. Simons, and B. Chambers for their assistance in programming and Drs. J. Miller and S. Lippard for samples of **2** and **3**, respectively. The experimental EXAFS measurements were made at the Stanford Synchrotron Radiation Laboratory with the financial support of the National Science Foundation under Contract DMR 77-27489 in cooperation with the U.S. Department of Energy.

Supplementary Material Available: Tables I–IV contain scattering amplitude and phase functions for carbon and oxygen and the least-squares refined fitting parameters for AB and ABC fits. Figures A and B contain best AB fits and parameter correlations for **1**–**3** (15 pages). Ordering information is given on any current masthead page.

Infrared Multiphoton Photochemistry of Vinylcyclopropane. Variation of Yield and Branching Ratio with Experimental Parameters

William E. Farneth,* Marcus W. Thomsen, Nancy L. Schultz, and Mark A. Davies

Contribution from the Department of Chemistry, The University of Minnesota, Minneapolis, Minnesota 55455. *Received October 27, 1980*

Abstract: The infrared photochemistry of vinylcyclopropane has been comprehensively investigated. Irradiation of vinylcyclopropane at relatively low pressures with the partially focused output of a CO_2 TEA laser leads to a mixture of the C_5 products cyclopentene, cyclopentadiene, 1,4-pentadiene, and *cis*- and *trans*-1,3-pentadiene. The composition of the product mixture as well as the total product yields are a sensitive function of experimental parameters. The effects of bath gas pressure, laser power, laser intensity, laser frequency, and number of pulses have been systematically examined. A simple physical picture of the multiphoton activation and resulting decomposition is developed. RRKM theory is employed to calculate energy-dependent unimolecular reaction rates. The model is quite successful in rationalizing these data, providing good evidence for the qualitative validity of a rate equation description of infrared multiphoton dissociation.

Dissociation of polyatomic molecules induced by multiphoton absorption in the infrared has a number of features that make it an attractive alternative to conventional activation methods for studying unimolecular reactions. It has been demonstrated that activation and dissociation can occur collisionlessly, over a microsecond or shorter timescale, and quite selectively for absorbing components in complex mixtures.[1-5] The general features of the mechanism by which individual molecules absorb the tens of photons required to reach dissociation thresholds are now fairly well understood. Models for this process commonly employ a rate equation approach.[6-9] It is postulated that activation occurs principally by sequential photon absorption. A partially activated molecule at any total internal energy may undergo further activation, deactivation, or chemical reaction with relative rates that are sensitive to reaction conditions. Much of the current interest in fundamental aspects of multiphoton activation comes from attempts to establish limits to the validity of such an approach and the specific form that rate constants of each of the three types should take.

It has been recognized for some time that reactant molecules that may decompose by more than one pathway can provide especially sensitive information relevant to these questions. Nevertheless, the number of studies which have investigated both yields and branching ratios as a function of systematic variation of reaction conditions have been relatively few.[10-15] Furthermore, in several cases one or both reaction pathways have yielded free radicals or other reactive fragments whose subsequent reactions complicate the analysis. We recently reported that multiphoton activation of vinylcyclopropane (vcp) leads to competitive isomerization reactions to four different, stable C_5H_8 products.[16] There

(1) Schulz, P. A.; Sudbo, Aa. S.; Krajnovich, D. J.; Kwok, H. S.; Shen, Y. R.; Lee, Y. T. *Annu. Rev. Phys. Chem.* **1979**, *30*, 379.
(2) Ambartzumian, R. V.; Letokhov, V. S. In "Chemical and Biochemical Applications of Lasers"; Moore, C. G., Ed.; Academic Press: New York, 1977; Vol. III.
(3) Rohn, A. M. *Sci. Am.* **1979**, *240*, 114.
(4) Cantrell, C. D.; Freund, S. M.; Lyman, J. L. In "Laser Handbook", North-Holland Publishing Co.: Amsterdam, 1978; Vol. III.
(5) Danen, W. C. *Opt. Eng.* **1980**, *19*, 21.
(6) Thiele, E.; Goodman, M. F.; Stone, J. *Opt. Eng.* **1980**, *19*, 10.
(7) Barker, J. R. *J. Chem. Phys.* **1980**, *71*, 3722.
(8) Quack, M. *J. Chem. Phys.* **1978**, *69*, 1282.
(9) Black, J. C.; Kolodner, P.; Schulz, M. J.; Yablonovitch, E.; Bloembergen, N. *Phys. Rev. A* **1979**, *19*, 704.
(10) Stephenson, J. C.; King, D. S. *Chem. Phys. Lett.* **1979**, *66*, 33.
(11) Colussi, A. F.; Benson, S. W.; Hwang, R. J.; Tiee, J. J. *Chem. Phys. Lett.* **1977**, *52*, 349.
(12) Rosenfeld, R. N.; Brauman, J. I.; Barker, J. R.; Golden, D. M. *J. Am. Chem. Soc.* **1977**, *99*, 8063.
(13) Brenner, D. M. *Chem. Phys. Lett.* **1978**, *57*, 357.
(14) Harrison, R. G.; Hawkins, H. L.; Leo, R. M.; John, P. *Chem. Phys. Lett.* **1980**, *70*, 555.
(15) Bucchele, J. L.; Weitz, E.; Lewis, T. D. *J. Am. Chem. Soc.* **1979**, *101*, 3700.

0002-7863/81/1503-4001$01.25/0